Solitary magnetic structures developed from gyro-resonance with solar wind ions at Mars and Earth

Li-Jen Chen[1], Jasper Halekas[2], Shan Wang[1,3], Gina A. DiBraccio[1], Norberto Romanelli[1,3], Jonathan Ng[1,3], Christopher T. Russell[4], Steven J. Schwartz[5,6], David Sibeck[1], William Farrell[1], Craig Pollock[7], Daniel Gershman[1], Barbara Giles[1], and Yaireska Collado-Vega[1]

[1] NASA Goddard Space Flight Center, Greenbelt, MD 20771

[2] University of Iowa, Iowa City, IA 52242

[3] University of Maryland, College Park, MD 20747

[4] University of California, Los Angeles, Los Angeles, CA 90095

[5] Laboratory for Space and Atmospheric Physics, Colorado University Boulder, Boulder, CO 80305

[6] Emeritus, Blackett Laboratory, Imperial College London, London SW7 2AZ, UK

[7] Denali Scientific, Healy, Alaska 99743

Key points

- Solitary magnetic structures with density enhancements, plasma heating, and ion reflection are observed in the Martian foreshock
- The structures resemble those developed from foreshock waves gyro-resonant with solar wind ions at Earth
- The structures and ion distributions are reproduced by simulations, and shown to be self-induced turbulence

Abstract

We investigate solitary magnetic structures in the foreshock of Mars and Earth. The structures exhibit pulse-like magnetic field and density enhancements along with plasma heating and local solar wind ion reflection. The structures at Mars resemble the foreshock structures developed from Ultra-Low-Frequency electromagnetic waves gyro-resonant with solar wind ions at Earth, and propagate toward the magnetosphere. We perform fully kinetic simulations to reproduce the solitary structures and the nonlinear evolution of ion distribution functions, illustrating their resonance with solar wind ions. The structures present self-induced foreshock turbulence that can have space weather effects. Our results advance the fundamental understanding of how solar wind interacts with planetary magnetospheres, and have potential impact on the current picture of planet-origin ion escape.

1. Introduction

Mars has an induced magnetosphere [Nagy et al., 2004; Ramstad et al., 2020], and a highly active environment upstream of the bow shock (e.g., review by Mazelle et al., 2004). The region upstream of the bow shock is permeated by a number of plasma waves, ranging from Alfvén waves [Dubinin et al., 2000; Halekas et al., 2017], Ultra-Low-Frequency (ULF) magnetosonic waves [Collinson et al., 2018; Ruhunusiri et al., 2016; Shan et al., 2020a] including those near the proton gyro-frequency [Brain et al., 2002; Russell et al., 1990; Romanelli et al., 2016], whistler-mode waves at frequencies of a few Hz [Brain et al., 2002; Halekas et al., 2020], and other higher frequency waves [Grard et al., 1989; Sagdeev et al., 1990; Skalsky et al., 1992]. Upstream particles, including reflected solar wind [Dubinin et al., 2006; Yamauchi et al., 2011] and freshly ionized Martian [Yamauchi et al., 2015a] protons as well as heavier ions [Yamauchi et al., 2015b] have been reported. A variety of structures have been observed upstream of the bow shock, including those identified as fast-mode small-scale shocks developed from ULF magnetosonic waves [Shan et al., 2020b], diamagnetic cavities [Øieroset et al., 2001], hot flow anomalies [Collinson et al., 2015], spontaneous hot flow anomalies [Collinson et al., 2017], foreshock cavities [Collinson et al., 2020], and quasi-periodic compressive structures reminiscent of Short Large Amplitude Magnetic Structures (SLAMS [Schwartz et al., 1992]) [Fowler et al., 2019; Halekas et al., 2017]. The ionospheric impact of ULF magnetosonic foreshock structures are documented [Collinson et al., 2018; Fowler et al., 2019]. Compressive foreshock structures have been shown to occur most frequently during times when the interplanetary magnetic field

(IMF) is nearly Sun-planet aligned (quasi-radial), but can occur under a broad range of upstream Mach number and dynamic pressure [Halekas et al., 2017].

In this paper, we analyze pulse-like magnetic field and density enhancements along with plasma distribution functions at Mars, compare them with structures from the Earth's foreshock with similar parameters, and elucidate the key defining physics with particle-in-cell (PIC) simulations. We term the pulses solitary magnetic structures because they exhibit properties (including polarization, spatial-temporal scales, capabilities to heat the plasma and reflect solar wind ions) similar to those developed from foreshock ULF waves gyro-resonant with solar wind ions at Earth [Chen et al., 2020; Paper I hereafter], in contrast with the ULF waves [Eastwood et al., 2005] gyro-resonant with backstreaming ions [Gary, 1991; Akimoto et al., 1993]. Intense solitary magnetic structures are shown by a global simulation of the terrestrial magnetosphere to bombard the magnetopause and induce reconnection as well as Earth-sized indents, opening potential dayside escape channels for planet-origin ions [Chen et al., 2021]. The induced magnetosphere of Mars, created by its ionosphere and crustal magnetic field, stands off the solar wind and produces a bow shock and magnetosheath that are much closer to the planet than those at Earth. We envision that the processes discussed in this paper have powerful capacities to facilitate dayside loss of Martian ions.

2. Spacecraft Measurements

In this section, we present examples of solitary magnetic structures from the foreshock of Mars and Earth, identify their similarities, and extract key parameters for simulations and linear instability analysis. The analyzed spacecraft measurements are from Mars Atmosphere and Volatile EvolutioN (MAVEN) [Jakosky et al., 2015] and Magnetospheric Multiscale (MMS) [Burch et al., 2016] missions. Two key parameters determining the dominant wave mode are: ratio of the density of ions streaming back toward the Sun (backstreaming, viewed in the plasma center-of-mass frame) to the total plasma density (n_b/n_0) and relative drift velocity (V_d/V_A) between the two ion populations [e.g., Gary, 1984; Akimoto et al., 1993; Weidl et al., 2019]. The selected MMS foreshock crossing has both parameters similar to those in the MAVEN event. MMS provides higher-resolution (~50 times higher cadence ion distribution functions than those from MAVEN, for example) plasma measurements to enable the ion phase space structure to be fully resolved and compared with simulation results.

The MAVEN measurements employed in this study are: magnetic field data (32 samples/s; 1 sample/s) from the Magnetometer [Connerney et al., 2015]; ion and electron energy flux (4 s per sample) and distribution functions (8 s per sample) from the Solar Wind Ion Analyzer (SWIA; Halekas et al., 2015) and the Solar Wind Electron Analyzer (SWEA; Mitchell et al., 2016), respectively; the plasma density data from the SWIA onboard moments (4 s per sample). Determination of the density and velocity of backstreaming protons in the foreshock region is based on data from both SWIA and the Supra-Thermal and Thermal Ion Composition (STATIC) instrument [McFadden et al., 2015]. All vector are shown in the Mars-Solar-Orbital (MSO) coordinate system in which the x-axis points from Mars to the Sun, the z-axis normal to the orbital plane (positive to the north), and the y-axis completes the right-handed coordinate system.

For the presented MMS data, the magnetic fields (128 samples/s) are measured by the Flux Gate Magnetometer [*Russell et al*., 2016], and electron (30 ms/sample) as well as ion (150 ms/sample for burst mode; 4.5 s/sample for fast survey mode) data from the Fast Plasma Investigation [*Pollock et al*., 2016]. Vectors are shown in the Geocentric solar ecliptic (GSE) coordinate system which is defined in an analogous manner as MSO.

Intense magnetic pulses (Figure 1c) disrupting the solar wind (Figure 1a) and heating electrons (Figure 1b) are observed upstream of the Martian bow shock (shown by the green shaded bar and orbit above Figure 1a and in Figure 1f, respectively) at ~1725-1830 UT on July 11, 2019. The IMF is dominantly Sun-Mars aligned with B_x much larger than $B_{y,z}$ as seen in the beginning of the shown interval (Figure 1e) and on average throughout the interval with magnetic pulses. The pulses reach magnitudes 10-18 nT ~5-9 times the background IMF strength (Figure 1c). Associated with the magnetic pulses are the plasma density enhancements to 4-5 cm^{-3} (the upstream solar wind density ~1.2 cm^{-3}, averaged from SWIA data at 1710-1720 UT). Solar wind protons exhibit strong deceleration at the magnetic field and density spikes, as seen by the intense flux extending from 1 keV to ~100 eV (Figures 1a and 2c). The nature of this deceleration will be further discussed in Figure 3.

The sudden disappearance of magnetic pulses at ~1830UT suggests a sharp boundary (at approximately Z ~ 1.2 R_M) beyond which the pulses are absent, rendering the primary impact region of the solitary structures to be the quasi-parallel foreshock within ~1R_M from the bow shock nose. Note that the IMF is still dominated by B_x and the ions are solar wind-like. The location of MAVEN at 1800 UT in MSO coordinates is [2.0, 0.4, 0.9]R_M, estimated to be ~0.5 R_M (~1695 km ~ 8 d_i, where d_i is the ion skin depth based on the upstream solar wind density) from the Martian bow shock encountered after 1840 UT (Figure 1a).

Similar to that which observed in the foreshock of Mars, disruption of the solar wind (Figure 1g) and heating of electrons (Figure 1h) are observed at the magnetic pulses in the selected MMS event. The magnetic field amplitude (Figure 1i) and plasma density (Figure 1j) are enhanced by about an order of magnitude compared with the upstream values (IMF ~ 4.1 nT; density ~ 3.7 cm^{-3}). The intense B_y and B_z (Figures 1e and 1k) exhibit both positive and negative excursions, and can enlarge magnetic shear angles across the magnetopause [Chen et al., 2021]. The MMS four spacecraft configuration in the selected foreshock crossing is colinear with an inter-spacecraft separation a few d_i, enabling definitive determination that the solitary magnetic structures evolve from the ULF waves gyro-resonant with solar wind ions (Figure 3 in Paper I).

For the wave gyro-resonant with solar wind ions, the inter-pulse separation results from the nature of the solitary pulse formation: growing from the maxima of beat-wave-like envelopes [Paper I], in contrast to the quasi-periodic shocks whose inter-pulse separation is dictated by the proton cyclotron periodicity [Shan et al., 2020b]. The separation in time between two consecutive pulses varies substantially, ranging from 5 to 25 s in the zoom-in interval (Figure 2f). For comparison, the proton cyclotron period for the background magnetic field (2 nT, taken from 1720 UT; MAVEN MAG) is ~33 s. The inter-pulse durations observed by MMS are also not organized by the cyclotron period which is ~17s for the MMS foreshock event (Figure 2n).

The backstreaming ion population exhibits a net sunward velocity in the spacecraft frame. The v_x reduced distribution function (summed over v_y and v_z; Figures 2b, 2d, and 2l) shows the colder solar wind population at v_x ~ -440 km/s, and the backstreaming hotter population (predominantly at v_x ~ 100-200 km/s in Figures 2b and 2l) which exhibits variations in both the phase-space-density (PSD) and velocity as does the backstreaming population in the simulation (Figures 3aeh).

We note the following additional features in the side-by-side zoom-in views of solitary magnetic structures from Mars and Earth shown in Figure 2: (1) At the solitary magnetic structures, the solar wind (SW) ion population is decelerated to below 100 eV as well as accelerated to ~4 keV (Figures 2c and 2k; the acceleration at Mars is further supported by H^+ data from STATIC). SW ion acceleration also occurs in the simulation (below -4 V_A in Figures 3h and 3n). (2) The most intense flux of decelerated SW ions occurs at the upstream edge of the structure (Figures 2cdg and 2klo; examples: 120131, 120220, and 120245 UT), corresponding to the density peak which tends to be displaced upstream from the magnetic field peak (Figure 2o; the structure at 120130 UT for example). (3) The duration of a single pulse is ~3-10 s (Figures 2f, 2j, and 2n; a 10s-duration pulse is at 183005-183015UT, not shown) and the pulse polarization is dominantly right-handed in the spacecraft frame (pulse moving toward -x, B_y leads B_z variations by ~90 degrees and B_x>0 in Figures 2f and 2n; magnetic wave power shown in Figures 2hi and 2pq), consistent with the polarization of ULF waves gyro-resonant with solar wind ions. (4) Electrons remain one population throughout the interval of interest (Figures 2e and 2m). The electron thermal spread in v_x enhances in intervals when thermalized ions are observed (Figures 2cde and 2klm; the interval at ~1821 UT for Mars, and 120120-30 UT for MMS) and the associated densities are relatively low.

We separate the solar wind and backstreaming populations in the 3D ion distribution data to compute their moments to obtain the key parameters needed for PIC simulations and linear instability analysis. For Mars, n_b/n_0 ~ 0.15-0.17, V_d/V_A ~ 15 based on

MAVEN data (SWIA and STATIC H+) from 20190711/1732-1734 UT. For Earth, n_b/n_0 ~ 0.17, V_d/V_A ~ 15 based on MMS3 data from 20190222/115819-20 UT. Solitary magnetic structures have been shown by PIC simulations to develop from ULF electromagnetic waves gyro-resonant with solar wind ions using a backstreaming ion density ratio n_b/n_0=0.5 extracted from an Earth foreshock event where N and |B| peaks coincide with each other without a relative phase shift [Paper I]. Using the same setup as in Paper I and the Mars/MMS parameters, the simulations reproduce structure properties including the displacement of the density peak slightly upstream of the |B| maximum as discussed below.

3. Particle-in-cell simulations

We carry out PIC simulations to demonstrate that given the conditions at the foreshock of Mars and Earth, intense solitary magnetic structures develop from waves gyro-resonant with solar wind ions under a constant IMF. The initial conditions are: two counterstreaming ion and one electron populations (as seen in Figures 2be and 2lm) with zero net total current. We perform simulations and corresponding linear instability analyses with n_b/n_0 = 0.1, 0.2 and V_d/V_A = 10, 15, 20. The mode gyro-resonant with solar wind ions dominates in all combinations of parameters in the above range. We show results from the run with n_b/n_0 = 0.2 and V_d/V_A = 20 to illustrate the key physics. In the plasma center-of-mass frame (plasma frame), the initial conditions are: one cold ion population moving at $V_{sw} = -4V_A$ (corresponding to $V_{sw} = -9V_A \sim -440\ km/s$ for Mars and Earth in the spacecraft frame), where V_A is the Alfvén speed based on the background magnetic field B_0 and the total number density (n_0); one hot backstreaming ion population at $V_b = 16V_A$; the temperature ratios $T_b/T_{sw} = 25$ and $T_e/T_{sw} = 2$; a uniform $B_0 = (0.067,0,0)m_e\, c/|e|d_e$, where m_e is the electron mass, c is the speed of light, e is the electron charge, and d_e is the electron inertia length. Other parameters are: the mass ratio $m_i/m_e = 100$, electron plasma to cyclotron frequency ratio $\omega_{pe}/\omega_{ce} = 15$, and solar wind ion beta $\beta = 1$. The simulation has one spatial and three velocity dimensions, performed using the particle-in-cell code VPIC, which solves a system of relativistic Vlasov-Maxwell equations [Bowers et al 2008].

In the simulation, the magnetic field $B_{y,z}$ grows from right-hand polarized electromagnetic waves (electric field variations are similar to those presented in Figures 2 and 4 in Paper I) in which B_y leads B_z by 90 degrees, consistent with the observed pulse forms shown in Figure 2. The magnetic field first develops as quasi-sinusoidal waves like the profiles from t-2 (Figure 3i; the even earlier stage is similar to that shown in Figure 4, Paper I). Later the field grows further at local maxima of |B| to form solitary structures at time t and t+2.5.

Simulation results show ion reflection, thermalization, and electron heating at sites of magnetic field and density enhancements, consistent with the observations (Figure 2) at the foreshock of Mars and Earth. Majorities of the incoming solar wind ions are reflected slightly upstream of the |B| peak, forming an arc structure in the [x, v_x] phase-space (Figure 3a). Such arc structures are seen in the high-cadence MMS ion v_x distribution (120130 and 120243 UT in Figure 2l). Electron heating occurs at the solitary structure, and tends to be more intense in regions where ions are more thermalized (e.g., x~580-585 in Figure 3b), similar to that observed by MAVEN and MMS (Figure 2).

The density (N) maximum is displaced slightly upstream (to the right) of the |B| peak (Figure 3d), a feature resolved by MMS (Figure 2o). At later time (for example, 2.5 ω_{ci}^{-1} later, where ω_{ci} is the ion cyclotron frequency), further ion thermalization occurs (Figure 3e), the magnetic field enhancements become more isolated (Figure 3f), and the relationship between the |B| and N peaks becomes more variable across different solitary structures (Figure 3g). The less correlated |B| and N profiles observed by MAVEN and MMS in the more thermalized regions (e.g., ~182050-182110 UT in Figures 2c and 2g for Mars; ~120120-120130 UT in Figures 2k and 2o for Earth) can thus be attributed to temporal evolution of the structures.

Solitary magnetic structures grow from waves gyro-resonant with solar wind ions. The mode is right-hand polarized and non-resonant with the backstreaming ions. Before the formation of solitary structures at time t, the wave propagates at $\mathbf{V}_{ph}$=-2V_A with a dominant wave number of kd_i~0.53, consistent with linear instability analysis predicting the maximum growth rate to be 0.81 ω_{ci} at kd_i~0.51 for the non-resonant mode. The cyclotron resonant velocity is $V_{res} = V_{ph} + \omega_{ci}/k = -3.9V_A$, within one solar-wind ion thermal speed (1.1 V_A) from $V_{sw} = -4V_A$, and hence satisfies the solar wind gyro-resonance condition [Gary, 1991; Weidl et al., 2019].

The capacity of solitary structures to reflect SW ions like a collisionless shock is further demonstrated by v_x-v_y ion velocity distribution functions (summed over $v_{z)}$ from PIC (Figure 3j), Mars (Figure 3k), and Earth (Figure 3l). All three distribution functions (in the spacecraft frame) show the co-existence of the slightly slowed down incoming SW and the reflected SW population at the upstream edge just before the |B| peak. The

v_x-v_y distributions are 2D velocity-space views of a slice (at a fixed x in PIC or fixed time in MMS) of the arc structure in the v_{ix} reduced distribution (Figures 2l and 3a).

The solitary-structure velocity lies between the incoming SW and the locally reflected SW populations, as verified by the PIC and MMS distributions. Based on MMS multi-spacecraft timing analysis, the propagation velocities of terrestrial solitary structures (such as the ones shown in Figure 2n) are estimated to be 200-300 km/s anti-sunward in the spacecraft frame, consistent with the average velocity of the incoming and reflected SW components (~ 5-6V_A ~ 250-300 km/s). For Mars, the observed velocities of the two populations indicate that the solitary structure moves toward the planet with a speed approximately 250-300 km/s.

Solitary magnetic structures are kinetic in nature. The solar wind ion population having a finite thermal spread in the velocity space enables gyro-resonance of a subset of SW ions with the wave and a rich spectrum of deceleration/acceleration (including reflections) throughout the solitary structure as seen in the x-v_x structure (Figure 3). To further illustrate this kinetic nature, we trace all SW ions within a spatial bin (size 0.02 d_i; marked by a magenta vertical line in Figure 3m) forward in time from t-2 (Figure 3m) to t, and display all traced ions (as magenta open circles) in the x-v_x phase-space at t (Figure 3n). The SW ions spread out from a 0.02 d_i bin to an x range of 13 d_i (x~600-613), occupy a much larger v_x range, and populate key x-v_x phase-space structures such as the arc (x~611-613; Figure 3n). Examination of traced solar wind ion orbits (one example shown as the cyan curve in Figure 3n) further confirms that reflection occurs at different locations within the solitary structure, and the most probable turning points correspond to the density peak. The histogram (Figure 3o) of the number of traced SW ions exhibits a profile qualitatively similar to the density profile (black curves in Figures 3m-n represents 3N). The differing acceleration and deceleration features of the SW ions and their local reflections throughout the magnetic structure indicate that the solar wind population cannot be viewed as a fluid element, but need to be treated as particles interacting through their mean fields.

4. Summary, discussion, and conclusion

In summary, we report solitary magnetic structures developed from gyro-resonance with solar wind ions in the foreshock of Mars, based on comparing MAVEN measurements with the high-cadence MMS data from an Earth foreshock crossing that exhibits similar parameters and comparing the observations with PIC simulations. The solitary structures in both observations and simulations decelerate/accelerate solar wind ions, locally reflect portions of the incoming solar wind population, and heat electrons, behaving like kinetic shocks moving toward the planet. The dominant instability is consistent with the right-hand non-resonant mode in the literature [Gary, 1991; Paper I], and requires higher backstreaming ion density and/or velocity than does the resonant mode. The evidence for the non-resonant mode reported in the paper indicates that a quasi-radial IMF may stimulate the foreshock/shock/magnetosphere environment of Mars to provide more/faster backstreaming ions through reflecting the incoming SW or through enabling ionized martian ions to flow sunward. The exact process remains an open question.

Strictly speaking, given the single spacecraft measurements from MAVEN, one cannot entirely rule out the possibility that the solitary structures are from the upstream solar wind and propagate to the foreshock of Mars. However, the presence of backstreaming ions, the similarity of structure properties with those observed in Earth's foreshock where the evolution of ULF waves into solitary structures are directly observed, and the similarity with solitary structures generated in PIC simulations all combine to support that the structures in the Martian foreshock are generated by the kinetic interaction of the solar wind and backstreaming ions.

The solitary magnetic structures discussed in this paper develop from the ULF electromagnetic waves gyro-resonant with solar wind protons (coded as "SWr structures" in this paragraph), to be distinguished from the periodic shocks that evolve from gyro-resonance with freshly ionized Martian hydrogen [Shan et al., 2020b]. The key observed differences are: 1) Polarization in the spacecraft frame: SWr structures are dominantly right-handed. The quasi-periodic shocks are primarily left-handed. 2) Time scales: for SWr structures, the inter-pulse duration is not organized by the cyclotron period, but as emphasized in Paper I, the solitary nature stems from a beat-like magnetic field envelope where the |B| local maxima set the initial locations for fastest nonlinear growth; the individual pulse span is 3-10 s, consistent with a time scale dominated by the Doppler shift $k\,V_{sw}/2\,\pi$ ~ 0.1-0.3 Hz (f_{ci} is only 0.03 Hz), where k is the most unstable wave number (kd_i~0.4-0.7) for the parameter range n_b/n_0 = 0.1-0.2 and V_d/V_A = 10-20. The quasi-periodic shocks are governed by the proton cyclotron periodicity. 3) Backstreaming ion velocity in the spacecraft frame: SWr structures are associated with ions streaming with a net sunward velocity. The backstreaming ion population for the quasi-periodic shocks are newborn protons that have a net anti-sunward velocity or nearly at rest [Shan et al., 2020b]. 4) Pulse shapes: SWr structures have bipolar B_{xyz} (the bipolar B_x with respect to the background field is most likely due to the wave vector not along x) dominated by B_{yz}. The B_{xyz} profiles of the quasi-periodic shocks are primarily unipolar (B_x never crosses zero, in particular; Figure 1b in Shan et al. [2020b]). Note that the above contrast is based on two case studies. Further investigations are required to assess the generality for both types of structures.

We emphasize that the physics leading to the density increase at the structures reported here is primarily local reflections of solar wind ions. Our simulation predicts that the most probable site of reflection corresponds to the density maximum, and occurs slightly upstream of the magnetic field peak given the parameters from the reported foreshock crossings at Mars and Earth. This displacement is observed by MMS in the high cadence measurements.

Solitary magnetic structures have the capacity to lead to dayside ion escape. The structures have been demonstrated to further intensify in the magnetosheath and lead to magnetic reconnection as well as indents at the magnetopause by a global hybrid simulation of the terrestrial magnetosphere [Chen et al., 2021]. The induced magnetosphere of Mars is much smaller and weaker than Earth's, and hence more susceptible to the impact of these planet-sized structures. For example, the foreshock generated and amplified bipolar B_y and B_z (Figures 2) can increase the shear angle between the magnetosheath field and the crustal magnetic field at the dayside, and hence may increase the likelihood of dayside reconnection such as that observed by MAVEN [Harada et al., 2018], and open escape pathways from the dayside ionosphere, a major reservoir of Martian ions. Even though the wave modes differ, the structures reported in this paper exhibit magnetic field and density enhancements similar in strengths as the

ULF magnetosonic waves (both types of structures can be viewed as subclasses of SLAMS [Schwartz et al., 1992], as they meet the criterion of |B| >~ $2B_0$), and hence may impact the ionosphere of Mars in ways similar to those documented [Collinson et al., 2018; Fowler et al., 2019] and contribute to the atmospheric loss.

In conclusion, the solitary magnetic structures in the foreshock of Mars are consistent with the terrestrial solitary structures developed from the ULF waves gyro-resonant with solar wind ions under a constant quasi-radial IMF. The structures are planet-sized and kinetic in nature, behaving like mini-shocks moving toward the magnetosphere. They have the potential to lead to dayside escape of planetary ions. Our results suggest that planet-sized space weather events can be self-induced under steady IMF and solar wind conditions.

Captions

Figure 1. Overview of solitary magnetic structures at the foreshock of Mars (left) and Earth (lower right). (a) Ion energy flux. (b) Electron energy flux. (c) Magnetic field amplitude enhanced with the density (d). (e) magnetic field components B_{xyz}. (f) MAVEN Orbit (color coded with shades of green along with the horizontal bar above Figure 1a to aid visualization). (g-k) Measurements from Earth's foreshock presented in the same format as Figures 1a-e.

Figure 2. Zoom-in view of example solitary structures and corresponding plasma distribution functions at Mars and Earth. (a, f, n) Magnetic field components. (b, d, l) Ion phase-space density in the v_x space (summed over v_y and v_z). (c, k) Ion energy flux. (e, m) Electron phase-space density in v_x. (g, o) pulse-like enhancements of the magnetic field amplitude and density. Ion thermalization (d, l) and electron heating (c, m) occur at solitary structures. (h-i, p-q) Magnetic wave power showing that the fluctuations at ~ 0.1Hz and slightly above are dominantly right-hand (RH) polarized, in contrast with the much weaker wave power in the LH panels. The vertical blue dashed lines mark the upstream side of example solitary structures and the center time of the distribution functions presented in Figure 3, magenta arrows example backstreaming ion populations when the SW is approximately un-disturbed, blue arrows example accelerated SW ion features, and black arrows the arc structures signifying local SW ion reflection.

Figure 3. PIC simulation results showing ion reflection, thermalization, and electron heating at sites of magnetic field and density enhancements, consistent with the observations at the foreshock of Mars and Earth. Local reflection of solar wind ions at the solitary structure is featured. (a-b, e, h) Ion and electron x-v_x phase space (summed over

v_y and v_z) presented in the plasma frame. (c, f, i) Magnetic field components showing $B_{y,z}$ develop from right-hand polarized waves. (d, g, m, o) Magnetic field amplitude (|B|) and density (N) profiles. Ion v_x-v_y velocity distribution functions from PIC (j), Mars (k), and Earth (l), presented in the same normalized unit, same velocity axes and velocity range in the spacecraft frame, showing that the incoming SW (denoted as "IncSW" and indicated by green arrows) co-exists with the locally reflected SW ("LocRefSW," magenta arrows). Zoom-in views of the SW ion x-v_x phase space at t-2 (m) and t (n) shows how all the solar wind ions in the 3D velocity distribution from x=615 (marked by a vertical magenta dashed line) at t-2 are distributed at t (magenta open circles). One example orbit of reflected SW ions is displayed as the cyan curve (n). The highest number of traced SW ions at time t (o) occurs at the location of the most probable reflection, corresponding to the bend-over location of the arc structure in x-v_x (n). (a-d) are from $t = 13$, (e-g) from $t + 2.5$, and (h-i) from $t - 2$. Time is in unit of ω_{ci}^{-1}. The horizontal green bar marks the x range shown in Figures 3m-o. The vertical line in (a-d) indicates the location from which the v_x-v_y distribution function (j) is taken.

Acknowledgments

The research at GSFC and UMCP is supported in part by the MMS mission, DOE grants DESC0016278, DESC0020058, NSF AGS-1619584, AGS-2010231, and NASA 80NSSC18K1369. N.R. is supported through a cooperative agreement with Center for Research and Exploration in Space Sciences & Technology II (CRESST II) between GSFC and UMCP under award number 80GSFC21M0002.

Open Research

MMS data are available at https://lasp.colorado.edu/mms/sdc/public/about/browse-wrapper/. MAVEN data are available at https://lasp.colorado.edu/maven/sdc/public/data/sci/. The study uses L2 FPI and FGM data from MMS, and L2 swi, swe, sta, and mag data from MAVEN.

References

Akimoto, K., Winske, D., Gary, S. P., and Thomsen, M. F. (1993), Nonlinear evolution of electromagnetic ion beam instabilities, J. Geophys. Res., 98 (A2), 1419– 1433, doi:10.1029/92JA02345.

Bowers, K. J., B. J. Albright, L. Yin, Bergen, and T. J. T. Kwan (2008), Ultrahigh performance three-dimensional electromagnetic relativistic kinetic plasma simulation, Phys. Plasmas, 15, 055,703

Brain, D. A., Bagenal, F., Acuña, M. H., Connerney, J. E. P., Crider, D. H., Mazelle, C., et al. (2002). Observations of low-frequency electromagnetic plasma waves upstream from the Martian shock. Journal of Geophysical Research: Space Physics, 107(A6), doi:10.1029/2000JD000416.

Burch, J. L. et al. (2016), Electron-scale measurements of magnetic reconnection in space, Science, 12, aaf2939.

Chen, L. J., Wang, S., Ng, J., Bessho, N., Tang, J. M., Fung, S. F., et al. (2020). Solitary magnetic structures at quasi-parallel collisionless shocks: Formation. Geophysical Research Letters, 48, e2020GL090800.

Chen, L.-J., Ng, J., Omelchenko, Y., & Wang, S. (2021). Magnetopause reconnection and indents induced by foreshock turbulence. Geophysical Research Letters, 48, e2021GL093029.

Collinson, G., Halekas, J., Grebowsky, J., Connerney, J., Mitchell, D., Espley, J., et al. (2015). A hot flow anomaly at Mars. Geophysical Research Letters, 42(21), 9121–9127. https://doi.org/10.1002/2015GL065079

Collinson, G., Sibeck, D., Omidi, N., Grebowsky, J., Halekas, J., Mitchell, D., et al. (2017). Spontaneous hot flow anomalies at Mars and Venus. Journal of Geophysical Research (Space Physics), 122(10), 9910–9923. https://doi.org/10.1002/2017JA024196

Collinson, G., Wilson, L. B., Omidi, N., Sibeck, D., Espley, J., Fowler, C. M., et al. (2018). Solar Wind Induced Waves in the Skies of Mars: Ionospheric Compression, Energization, and Escape Resulting From the Impact of Ultralow Frequency Magnetosonic Waves Generated Upstream of the Martian Bow Shock. Journal of Geophysical Research (Space Physics), 123(9), 7241–7256. https://doi.org/10.1029/2018JA025414

Collinson, G., Sibeck, D., Omidi, N., Frahm, R., Zhang, T., Mitchell, D., et al. (2020). Foreshock Cavities at Venus and Mars. Journal of Geophysical Research: Space Physics, 125(8), e2020JA028023. https://doi.org/10.1029/2020JA028023

Connerney, J., Espley, J., Lawton, P., Murphy, S., Odom, J., Oliversen, R., & Sheppard, D. (2015). The MAVEN magnetic field investigation. Space Science Reviews, 195, 257–291. https://doi.org/10.1007/s11214-015-0169-4

Dubinin, E., Sauer, K., Delva, M., Livi, S., Lundin, R., Skalsky, A., & Szego, K. (2000). Deceleration of the Solar Wind Upstream of the Martian Bow Shock. Mass-loading or Foreshock Features? Advances in Space Research, 26(10), 1627–1631. https://doi.org/10.1016/S0273-1177(00)00104-6

Dubinin, E., Fraenz, M., Woch, J., Barabash, S., Lundin, R., & Yamauchi, M. (2006). Hydrogen exosphere at Mars: Pickup protons and their acceleration at the bow shock. Geophysical Research Letters, 33(22), L22103. https://doi.org/10.1029/2006GL027799

Eastwood, J. P., Balogh, A., Lucek, E. A., Mazelle, C., & Dandouras, I. (2005). Quasi-monochromatic ULF foreshock waves as observed by the four-spacecraft cluster mission: 1. Statistical properties. Journal of Geophysical Research, 110, A11219. https://doi.org/10.1029/2004JA010617

Fowler, C. M., Halekas, J., Schwartz, S., Goodrich, K. A., Gruesbeck, J. R., & Benna, M. (2019). The Modulation of Solar Wind Hydrogen Deposition in the Martian Atmosphere by Foreshock Phenomena. Journal of Geophysical Research: Space Physics, 124(8), 7086–7097. https://doi.org/10.1029/2019JA026938

Gary, S. P. (1991), Electromagnetic ion/ion instabilities and their consequences in space plasmas—A review, Space Sci Rev., 56, 373–415, doi:10.1007/BF00196632.

Grard, R., Pedersen, A., Klimov, S., Savin, S., Skalsky, A., Trotignon, J. G., & Kennel, C. (1989). First measurements of plasma waves near Mars. Nature, 341(6243), 607–609. https://doi.org/10.1038/341607a0

Halekas, J. S., Taylor, E. R., Dalton, G., Johnson, G., Curtis, D. W., McFadden, J. P., Mitchell, D. L., Lin, R. P., and Jakosky, B. M. (2015), The solar wind ion analyzer for MAVEN, Space Sci. Rev., doi:10.1007/s11214-013-0029-z

Halekas, J. S., Ruhunusiri, S., Harada, Y., Collinson, G., Mitchell, D. L., Mazelle, C., et al. (2017). Structure, dynamics, and seasonal variability of the Mars-solar wind interaction: MAVEN Solar Wind Ion Analyzer in-flight performance and science results. Journal of Geophysical Research (Space Physics), 122(1), 547–578. https://doi.org/10.1002/2016JA023167

Halekas, J. S., Ruhunusiri, S., Vaisberg, O. L., Harada, Y., Espley, J. R., Mitchell, D. L., et al. (2020). Properties of Plasma Waves Observed Upstream From Mars. Journal of Geophysical Research: Space Physics, 125(9), e2020JA028221. https://doi.org/10.1029/2020JA028221

Harada, Y., Halekas, J. S., DiBraccio, G. A., Xu, S., Espley, J., McFadden, J. P., et al. (2018). Magnetic reconnection on dayside crustal magnetic fields at Mars: MAVEN observations. Geophysical Research Letters, 45, 4550–4558. https://doi.org/10.1002/2018GL077281

Jakosky, B. M., et al. (2015), The Mars Atmosphere and Volatile Evolution (MAVEN) mission, Space Sci. Rev., doi:10.1007/s11214-015-0139-x.

Le, G., C. T. Russell, M. F. Thomsen, and J. T. Gosling (1992), Observations of a new class of upstream waves with periods near 3 seconds, J. Geophys. Res., 97, 2917–2925.

Mazelle, C., Winterhalter, D., Sauer, K., Trotignon, J. G., Acuña, M. H., Baumgärtel, K., et al. (2004). Bow Shock and Upstream Phenomena at Mars. Space Science Reviews, 111(1), 115–181. https://doi.org/10.1023/B:SPAC.0000032717.98679.d0

McFadden, J. P., Kortmann, O., Curtis, D., Dalton, G., Johnson, G., Abiad, R., et al. (2015). MAVEN SupraThermal and Thermal Ion Composition (STATIC) instrument. Space Science Reviews, 195(1-4), 199–256. https://doi.org/10.1007/s11214-015-0175-6

Mitchell, D. L., Mazelle, C., Sauvaud, J.-A., Thocaven, J.-J., Rouzaud, J., Fedorov, A., et al. (2016). The MAVEN Solar Wind Electron Analyzer. Space Science Reviews, 200, 495–528. https://doi.org/10.1007/s11214-015-0232-1

Nagy, A. F., Winterhalter, D., Sauer, K., Cravens, T. E., Brecht, S., Mazelle, C., et al. (2004). The plasma environment of Mars. Space Science Reviews, 111(1/2), 33–114. https://doi.org/10.1023/B:SPAC.0000032718.47512.92

Øieroset, M., Mitchell, D. L., Phan, T. D., Lin, R. P., & Acuña, M. H. (2001). Hot diamagnetic cavities upstream of the Martian bow shock. Geophysical Research Letters, 28(5), 887–890. https://doi.org/10.1029/2000GL012289

Pollock, C., Moore, T., Jacques, A., Burch, J., Gliese, U., Saito, Y., et al. (2016). Fast plasma investigation for magnetospheric multiscale. Space Science Reviews, 199, 331–406. https://doi.org/10.1007/s11214-016-0245-4

Romanelli, N., et al. (2016), Proton cyclotron waves occurrence rate upstream from Mars observed by MAVEN: Associated variability of the Martian upper atmosphere, J. Geophys. Res. Space Physics, 121, doi:10.1002/2016JA023270

Ramstad, R., Brain, D.A., Dong, Y. et al. (2020). The global current systems of the Martian induced magnetosphere. Nat Astron 4, 979–985. https://doi.org/10.1038/s41550-020-1099-y

Ruhunusiri, S., Halekas, J. S., Connerney, J. E. P., Espley, J. R., McFadden, J. P., Mazelle, C., et al. (2016). MAVEN observation of an obliquely propagating low-frequency wave upstream of Mars. Journal of Geophysical Research (Space Physics), 121(3), 2374–2389. https://doi.org/10.1002/2015JA022306

Russell, C. T., Luhmann, J. G., Schwingenschuh, K., Riedler, W., & Yeroshenko, Ye. (1990). Upstream waves at Mars: Phobos observations. Geophysical Research Letters, 17(6), 897–900. https://doi.org/10.1029/GL017i006p00897

Russell, C. T., Anderson, B. J., Baumjohann, W., Bromund, K. R., Dearborn, D., Fischer, D., et al. (2016). The magnetospheric multiscale magnetometers. Space Science Reviews, 199, 189–256. https://doi.org/10.1007/s11214-014-0057-3

Sagdeev, R. Z., Shapiro, V. D., Shevchenko, V. I., Zacharov, A., Király, P., Szegó, K., et al. (1990). Wave activity in the neighborhood of the bowshock of Mars. Geophysical Research Letters, 17(6), 893–896. https://doi.org/10.1029/GL017i006p00893

Schwartz, S. J., D. Burgess, W. P. Wilkinson, R. L. Kessel, M. Dunlop, and H. Luehr (1992), Observations of short large-amplitude magnetic structures at a quasi-parallel shock, J. Geophys. Res., 97, 4209–4227, doi:10.1029/91JA02581.

Skalsky, A., Grard, R., Klimov, S., Nairn, C. M. C., Trotignon, J. G., & Schwingenschuh, K. (1992). The Martian bow shock: Wave observations in the upstream region. Journal of Geophysical Research: Space Physics, 97(A3), 2927–2933. https://doi.org/10.1029/91JA03078

Shan, L., Ge, Y., & Du, A. (2020a). A case study of large-amplitude ULF waves in the Martian foreshock. Earth and Planetary Physics, 4(1), 45–50. https://doi.org/10.26464/epp2020004

Shan, L., Tsurutani, B. T., Ohsawa, Y., Mazelle, C., Huang, C., Du, A., et al. (2020b). Observational Evidence for Fast Mode Periodic Small-scale Shocks: A New Type of Plasma Phenomenon. The Astrophysical Journal Letters, 905(1), L4. https://doi.org/10.3847/2041-8213/abcb02

Weidl, M. S., Winske, D., and Niemann, C. (2019), On the background-gyroresonant character of Bell's instability in the large-current regime, The Astrophys. J., 872:48, https://doi.org/10.3847/1538-4357/aafad0.

Yamauchi, M., Futaana, Y., Fedorov, A., Frahm, R. A., Winningham, J. D., Dubinin, E., et al. (2011). Comparison of accelerated ion populations observed upstream of the bow shocks at Venus and Mars. Annales Geophysicae, 29(3), 511–528. https://doi.org/10.5194/angeo-29-511-2011

Yamauchi, M., Hara, T., Lundin, R., Dubinin, E., Fedorov, A., Sauvaud, J.-A., et al. (2015a). Seasonal variation of Martian pick-up ions: Evidence of breathing exosphere. Planetary and Space Science, 119, 54–61. https://doi.org/10.1016/j.pss.2015.09.013

Yamauchi, M., Lundin, R., Frahm, R. A., Sauvaud, J.-A., Holmström, M., & Barabash, S. (2015b). Oxygen foreshock of Mars. Planetary and Space Science, 119, 48–53. https://doi.org/10.1016/j.pss.2015.08.003

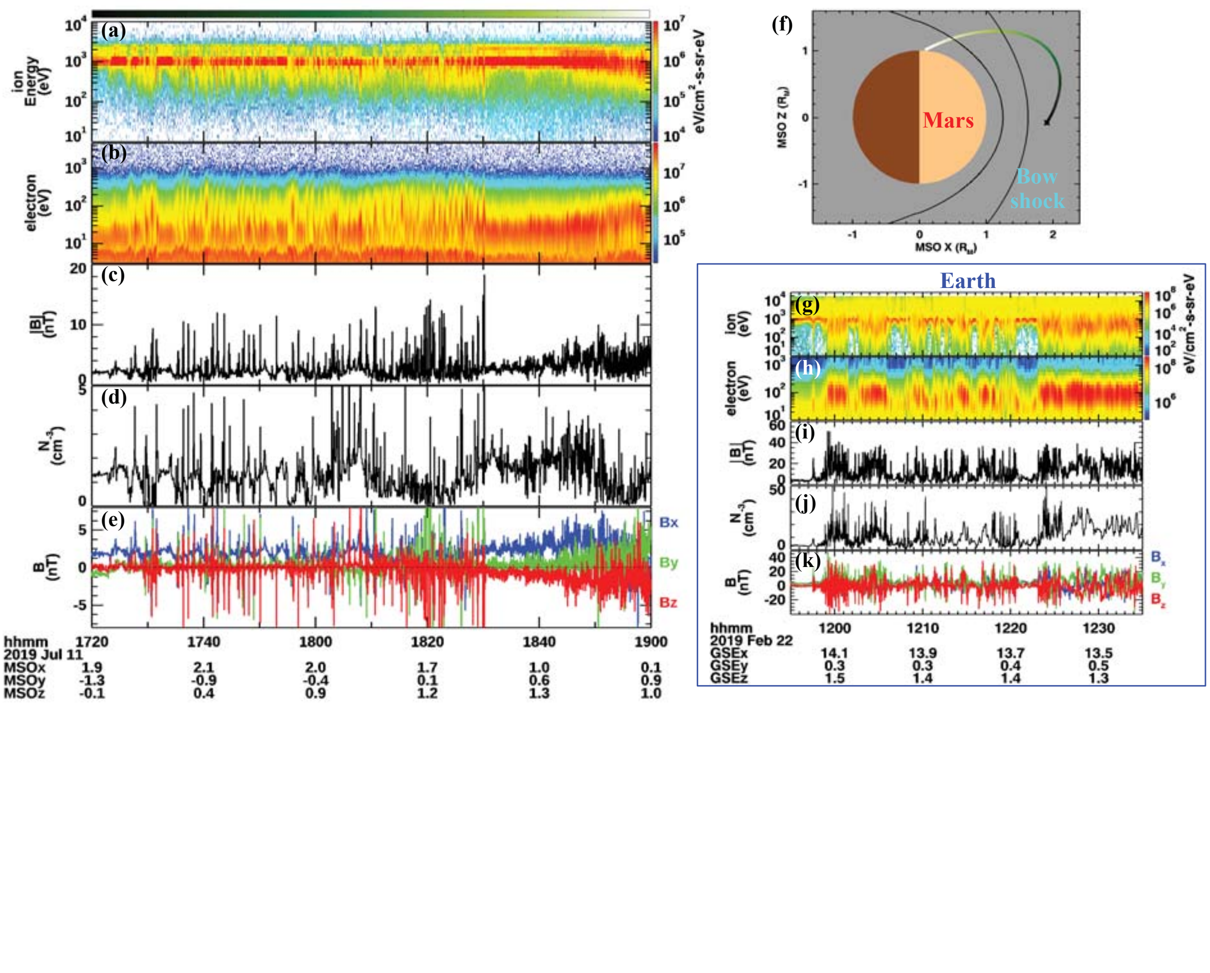
(a)
ion Energy (eV)
eV/cm^2-s-sr-eV
(b)
electron (eV)
(c)
|B| (nT)
(d)
N (cm^{-3})
(e)
B (nT)
Bx
By
Bz
hhmm 1720 1740 1800 1820 1840 1900
2019 Jul 11
MSOx 1.9 2.1 2.0 1.7 1.0 0.1
MSOy -1.3 -0.9 -0.4 0.1 0.6 0.9
MSOz -0.1 0.4 0.9 1.2 1.3 1.0
(f)
Mars
Bow shock
MSO X (R_M)
MSO Z (R_M)
Earth
(g)
(h)
(i)
(j)
(k)
hhmm 1200 1210 1220 1230
2019 Feb 22
GSEx 14.1 13.9 13.7 13.5
GSEy 0.3 0.3 0.4 0.5
GSEz 1.5 1.4 1.4 1.3

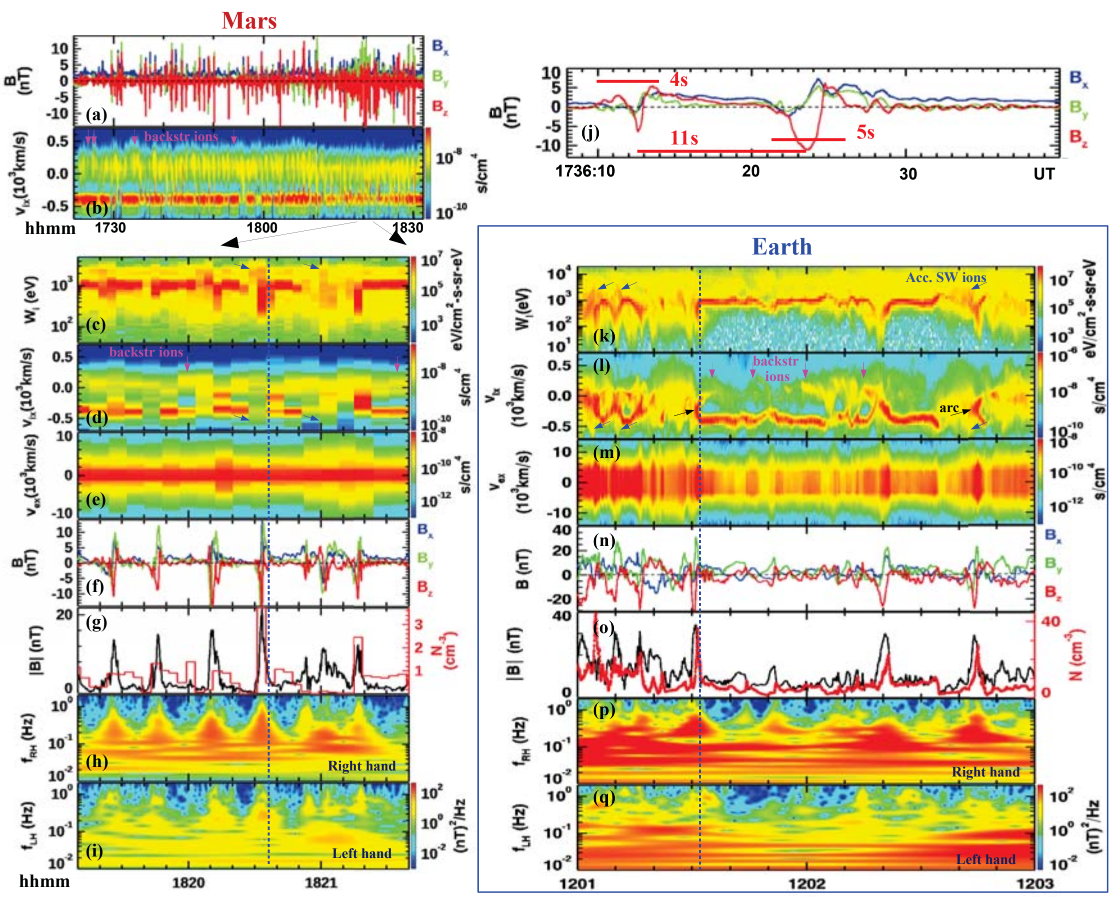
Mars
Earth
(a) (b) (c) (d) (e) (f) (g) (h) (i)
(j)
(k) (l) (m) (n) (o) (p) (q)
B (nT)
B_x B_y B_z
backstr ions
$v_{ix}(10^3 km/s)$
s/cm^4
hhmm 1730 1800 1830
W_i (eV)
eV/cm^2-s-sr-eV
$v_{ex}(10^3 km/s)$
|B| (nT)
N (cm^{-3})
f_{RH} (Hz)
Right hand
f_{LH} (Hz)
Left hand
(nT)^2/Hz
hhmm 1820 1821
4s
11s
5s
1736:10 20 30 UT
Acc. SW ions
backstr ions
arc
1201 1202 1203

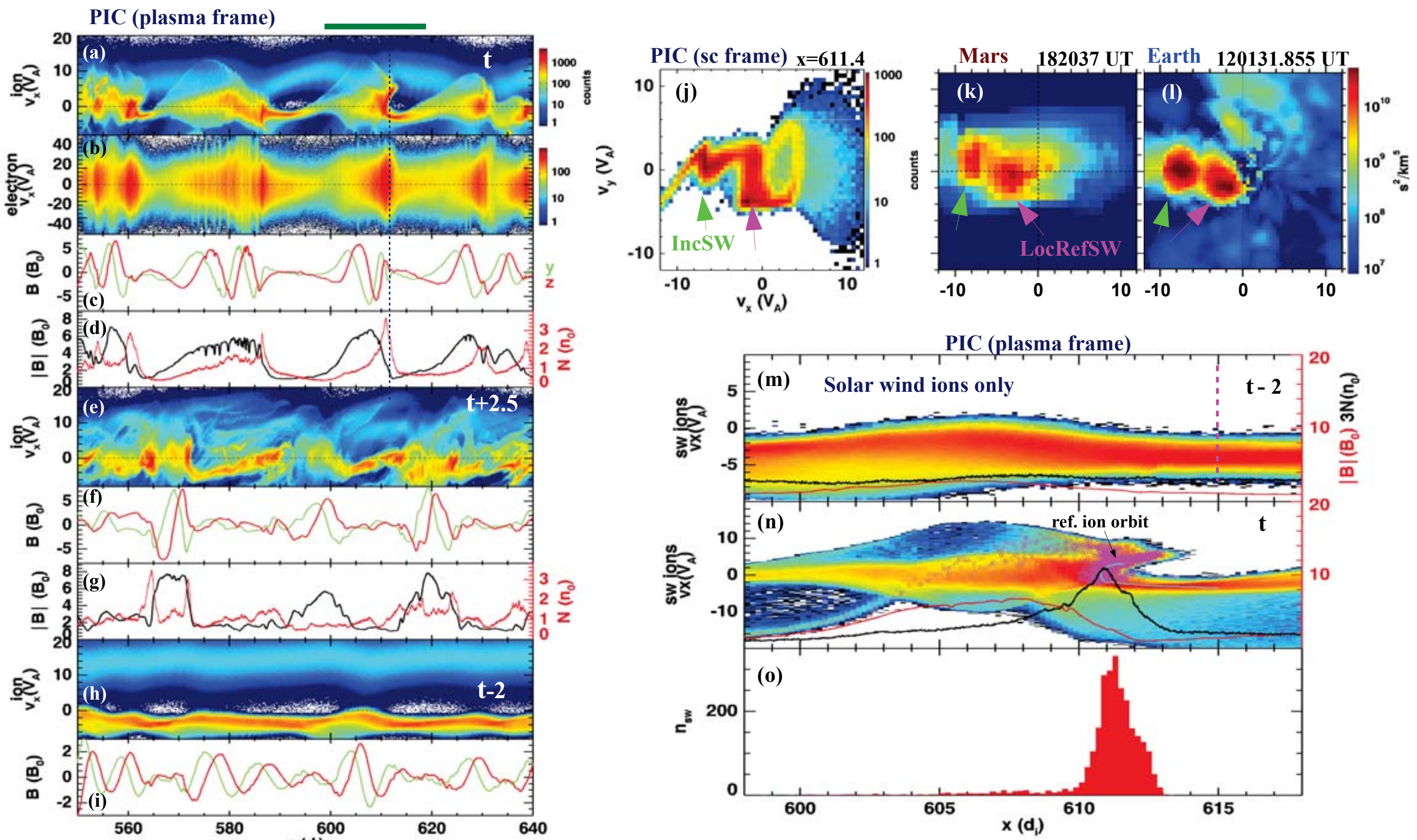

PIC (plasma frame)
(a)
t
ion v_x (V_A)
counts
(b)
electron v_x (V_A)
(c)
B (B_0)
y
z
(d)
|B| (B_0)
N (n_0)
(e)
t+2.5
(f)
(g)
(h)
t-2
(i)
x (d_i)
PIC (sc frame)
x=611.4
(j)
v_y (V_A)
v_x (V_A)
IncSW
Mars
182037 UT
Earth
120131.855 UT
(k)
(l)
LocRefSW
s^2/km^3
PIC (plasma frame)
(m)
Solar wind ions only
t - 2
sw ions vx(V_A)
|B|(B_0) 3N(n_0)
(n)
ref. ion orbit
t
(o)
n_{sw}
x (d_i)